J Mol Model (2007) 13: 1–10
DOI 10.1007/s00894-006-0112-4

ORIGINAL PAPER

Balázs Jójárt · Árpád Márki

Possible dynamic anchor points in a benzoxazinone derivative–human oxytocin receptor system — a molecular docking and dynamics calculation

Received: 16 December 2005 / Accepted: 15 February 2006 / Published online: 5 May 2006

Abstract In this study, we performed a molecular docking and dynamics simulation for a benzoxazinone–human oxytocin receptor system to determine the possible hydrophobic and electrostatic interaction points in the dynamic complex. After the homology modeling, the ligand was docked into the putative active using AutoDock 3.05. After the application of energetic and structural filters, the complexes obtained were further refined with a simulated annealing protocol (AMBER8) to remove steric clashes. Three complexes were selected for subjection to the molecular dynamics simulation (5 ns), and the results on the occurrence of average anchor points showed a stable complex between the benzoxazinone derivative and the receptor. The complex could be used as a good starting point for further analysis with site-directed mutagenesis, or further computational research.

Keywords Oxytocin receptor · Non-peptide antagonist · Homology model · Molecular docking · Molecular dynamics

Abbreviations OTR: Oxytocin receptor · OT: Oxytocin · hOTR: Human oxytocin receptor · MD: Molecular dynamics · BZX: Benzoxazinone · GPCRs: G-protein coupled receptors · TM: Transmembrane · SA: Simulated annealing · bRho: Bovine rhodopsin · RMSD: Root-mean-square distance · GAFF: General Amber Force Field · ΔG_{bind}: Estimated free energy of binding · EC: Extracellular · IC: Intracellular

Electronic Supplementary Material Supplementary material is available at http://dx.doi.org/10.1007/s00894-006-0112-4

B. Jójárt (✉) · Á. Márki
Department of Pharmacodynamics and Biopharmacy,
University of Szeged,
Eötvös u. 6,
6721 Szeged, Hungary
e-mail: jojartb@pharm.u-szeged.hu
Tel.: +36-62-545567
Fax: +36-62-545567

Introduction

In recent years, the oxytocin receptor (OTR) has been detected in various tissues, such as cancer [1] and endothelial cells [2], cardiomyocytes [3], myoblasts [4], and bone cells [5]. Nevertheless, it has been confirmed that the main role of the peptide neurohypophyseal hormone oxytocin (OT) is to induce uterine contractions during parturition and milk ejection during lactation. This effect on the uterus is the basis of its pharmacological use because inhibition of the receptorial effect of OT is a logical alternative to tocolysis. The peptide atosiban (Tractocile [6]) is still in clinical use [7] but can be administered only parenterally. A number of research groups accordingly have recently investigated the synthesis, pharmacological characterization, and molecular interaction modeling of non-peptide OTR antagonists [8–11].

With the aid of molecular modeling and site-directed mutagenesis analysis, Hawtin et al. [12] identified an anchor point in the human OTR–benzoxazinone (hOTR–BZX) complex, i.e., the hydrophobic residue Ala318, which can interact with the methoxy group of L-371,257 and L-372,662, which are non-peptide antagonists, containing the BZX basic structure. In an earlier article [13], we described the most likely active conformation of the complexes formed between hOTR and 45 BZX analogues taken from the literature [14, 15]. The most active benzoxazinone analogue was docked into the putative active site, and further refinement protocol, scoring functions and three-dimensional (3D)-QSAR methods were used to identify the most likely active conformation. The Ala318 interaction point was also determined later in our complex and indicated that the complex could be suitable for the study of receptor–ligand complexes. However, there are some disadvantages of the model: (1) the hOTR model was constructed on the basis of a δ-opioid receptor template; (2) we used a truncated receptor model (all receptor residues closer than 10 Å to the ligands were retained, and the remainder were deleted from the model); (3) the receptor flexibility was taken into account only in the refinement procedure to remove the

steric clashes; and, finally, (4) the stability of the complex was not tested via a molecular dynamics (MD) simulation. Therefore, the aims of the present study were as follows: (1) construction of a relevant 3D model of the hOTR; (2) possible active-conformation generation by using the most active compound (BZX, Fig. 1) [14, 15]; and (3) complex stability investigation by means of a MD simulation.

Materials and methods

Homology modeling

On the assumption that G-protein coupled receptors (GPCRs) share similar transmembrane (TM) boundaries and overall topology, a homology model of the hOTR was constructed from the ground-state crystal structure of bovine rhodopsin (bRho) (PDB access number 1F88) [16]. The alignment was taken from the literature (the overall sequence identity between hOTR and bRho is about 48% when identical residues and conserved substitutions are taken into account [12]).

The homology modeling was performed by means of the homology modeling module of the MOE 2004.03 [17] program package. After the sequence alignment, 100 structures were generated, and the average structure was selected for further refinement. Only 12 residues from the N-terminal (Arg27–Leu38) and 16 residues (Leu333–Ser348) directly following the TM7 were included in the models; the final model accordingly consists of 322 amino acids. The structure was minimized with the help of the steepest descent, the conjugated gradient, and, finally, the truncated Newton methods in a consecutive manner; the gradients were 100, 10, and 0.001, respectively. The Amber94 force field [18] was used with MOE 2004.03.

After the minimization, the minimized structure was refined further with simulated annealing (SA), using the AMBER8 [19] program package. The SA protocol was as follows: the structure was heated to 600 K in 8 ps, equilibrated at 600 K for 20 ps, and cooled down to 50 K in 10 ps; the structure obtained was minimized (10,000 cycles). During the protocol, the α-carbons of the whole protein were restrained to their initial positions with a 150-kcal mol^{-1} Å^{-2} force constant. The temperature coupling constants 0.5, 1, and 0.5 ps were used in the heating, equilibration, and cooling stage, respectively, and bonds involving H atoms were also constrained using the SHAKE algorithm. During the calculations, a distance-dependent dielectric constant (ε_r=4) and a 30-Å cutoff were used for the long-range non-bonded interactions. This cycle was repeated 50 times, and the structure with the lowest energy was subjected to docking calculations.

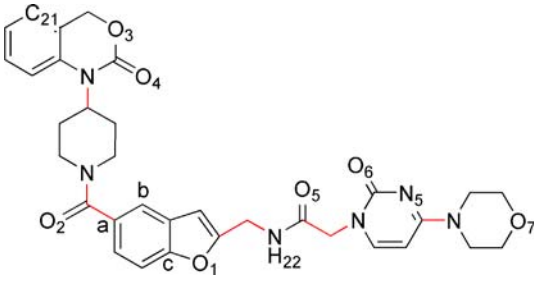

Fig. 1 The structure of the docked compound. Red bonds proved flexible during the docking calculation (AutoDock 3.05 [20]). The atoms denoted by *a*, *b*, and *c* are those used in the reorientation (*a*, *b*, *c* and *c*, *b*, *a*) procedure during the RESP calculation with RED-vII [25]

Docking protocol

The BZX analogue, with high affinity toward the hOTR (pK_i=9.3 [15], Fig. 1) was docked into the receptor model, using the AutoDock 3.05 software [20]. The initial structure of the analogue was prepared in MOE 2004.03 and was minimized (grad <0.001) using the MMFF94 force field [21].

As AutoDock 3.05 allows only one of the docking partners to be flexible, the receptor was kept rigid, and the ligand was allowed to be flexible. The grid box (52×60×78 grid points) was centered on the putative active site, and the lattice point distance was set to 0.375 Å. Lennard–Jones parameters 12–10 and 12–6 were used for the modeling of H-bonds and van der Waals interactions, respectively. In calculations of the electrostatic grid map (Gasteiger and united Kollman charges for the ligand and the receptor, respectively), the distance-dependent dielectric constant of Mehler and Solmayer was used [22]. During the docking procedure, the Lamarckian genetic algorithm with the pseudo-Solis and Wets method was used, with 250 individuals in the population. The stopping criterion was defined by the total number of energy evaluations, which was set to 5×10^7. The translation step was set to 0.5 Å/step, and in both quaternion and torsion steps, 5.0 degrees/step was used. In one docking calculation, 50 structures were generated, and this was repeated ten times (500 structures) to obtain good conformational sampling.

In the filtration of the structures and to confirm the complexes formed by means of theoretical calculations, we calculated the free energy of binding (ΔG_{bind}) using the scoring function implemented in AutoDock 3.05. This empirical scoring function includes five terms: van der Waals (Lennard–Jones 12–6 potential), H-bond (Lennard–Jones 12–10 potential), screened Coulombic electrostatic potential and solvation terms, and one ligand flexibility-including term. The coefficients of the five terms were determined by linear regression, using 30 protein–ligand complexes [20].

To determine possible initial complexes, we used the following filters: (1) the estimated ΔG_{bind} should be less than 1,000 kcal mol^{-1}; (2) our previous results and those of Hawtin et al. [12] indicated that the compounds bind in an extended conformation to the putative active site of the hOTR, and we, therefore, used a distance filter, *d*(C21–O7) <15 Å (Fig. 1), to remove the non-relevant structures. On use of these two filters, the number of possible structures decreased from 500 to 129. A further filter was also

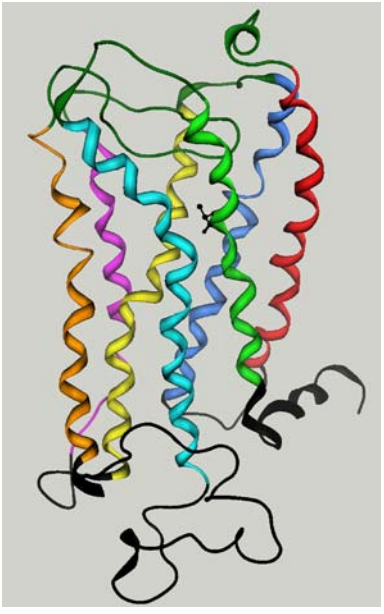

Fig. 2 The structure of the hOTR after the homology modeling. The Ala318 residue is depicted (*ball and stick*), which was determined by Hawtin et al. [12]. TM1, *red*; TM2, *blue*; TM3, *yellow*; TM4, *violet*; TM5, *orange*; TM6, *cyan*; TM7, *green*. The extracellular loops are colored *dark green*, and the intracellular loops *black*

applied: the presence of the hydrophobic interaction point Ala318 (Fig. 2).

The interacting hydrophobic residues were determined by means of LIGPLOT v4.4.2 [23]. The 18 possible complexes determined were further refined with the same SA protocol as described earlier, except that ten cycles were performed for each complex.

For the ligand, the General Amber Force Field (GAFF) [24] was used. The charges of the ligand were calculated using the multi-conformer, multi-orientation RESP calculation implemented in the R.E.D. II software [25], using the Gaussian03 quantum mechanical program [26]. Three complexes were selected randomly from the docked structures and were subjected to the calculation; the re-orientation was based on the three atoms denoted by a, b, and c in Fig. 1.

Table 1 The predicted free energy of binding (kcal mol^{-1}) for complexes A, B, C, D, E, and F before force field minimization ($\Delta G_{bind,i}$, using a rigid receptor), after force field minimization ($\Delta G_{bind,f}$), and after the SA protocol, using the lowest energy structure ($\Delta G_{bind,SA}$)

ID	$\Delta G_{bind,i}$	$\Delta G_{bind,f}$	$\Delta G_{bind,SA}$
A	462.3	−22.9	−25.1
B	516.1	−23.3	−23.6
C	525.5	−23.4	−23.7
D	670.3	−25.1	−24.5
E	700.9	−24.0	−24.4
F	795.8	−23.7	−24.0

The ΔG_{bind} values were calculated by using the built-in scoring function of AutoDock 3.05 [20]

Molecular dynamics simulation

The MD simulation was performed by using the AMBER8 program suite. For the protein and the ligand, the Amber94 force field and GAFF, respectively, were used. The system was heated in a multi-step heating protocol: the temperature was increased from 0 K to 300 K in five steps (ΔT=60 K, Δt=10 ps); the time step was set to 0.5 fs. After the heating, the system was equilibrated at 300 K for 5 ns, the time step was set to 2 fs, and the SHAKE algorithm was used to constrain bonds involving hydrogen. The αC atoms of the transmembrane regions were restrained to their initial positions with a 5 kcal mol^{-1} $Å^{-2}$ force constant.

Results and discussion

After the homology model building and refinement, the 3D hOTR model obtained was tested via the MOE/protein report module. No significant differences were obtained as compared with the values published by Laskowski et al.

Table 2 The evolved hydrophobic interactions determined for complexes B, E, and F with the LIGPLOT software [23]

Complex B	Complex E	Complex F
–	Leu74	–
Phe77	Phe77	–
Met78	Met78	Met78
Leu81	Leu81	Leu81
Val88	Val88	Val88
Gln92	–	Gln92
Val93	–	–
Gln119	Gln119	Gln119
–	–	Gly122
Met123	Met123	Met123
Ser126	Ser126	Ser126
Thr127	–	Thr127
Leu129	–	–
Leu130	Leu130	Leu130
Met133	Met133	Met133
Phe185	–	–
Asp186	–	–
Met276	–	–
–	–	Thr277
Ile280	Ile280	Ile280
–	–	Ala283
Phe284	Phe284	Phe284
Cys287	Cys287	Cys287
–	–	Trp288
Ala318	Ala318	Ala318
Ser319	Ser319	Ser319
Asn321	Asn321	Asn321
–	–	Ser322
Asn325	–	–
Ile328	–	–
Tyr329	–	Tyr329

Table 3 Possible electrostatic interactions in complex B

Complex ID	Interacting atoms	d(A···D)/Å	α(A···H–D)/°
Complex B	L_O3···Val93_H	5.28	123.6
	L_O3···Gly122_H	5.00	115.8
	L_O3···Ser319_HG	5.17	44.6
	L_O4···Gly122_H	3.46	106.5
	L_O4···Met123_H[a]	2.80	93.8
	L_O4···Asn321_HD21	4.45	64.9
	L_O4···Asn321_HD22	3.65	110.9
	L_O2···Trp288_H	4.23	75.2
	L_O2···Trp288_HE1	6.66	34.2
	L_O1···Ser126_HG	3.83	95.1
	L_O1···Phe284_H	3.61	94.4
	L_O1···Asn325_HD21	4.63	119.2
	L_O1···Asn325_HD22	6.20	8.8
	L_H22···Ser126_OG	3.52	151.1
	L_H22···Asn325_OD1	4.32	134.9
	L_O5···Leu129_H	5.00	91.9
	L_O5···Leu130_H	3.56	61.9
	L_O6···Hip80_HD1	4.64	133.6
	L_N5···Leu81_H	4.99	124.3
	L_O7···Tyr329_H	3.12	73.6
Complex E	L_O4···Gly122_H	3.81	106.7
	L_O4···Met123_H[a]	2.99	100.5
	L_O4···Asn321_HD21	4.45	64.1
	L_O4···Asn321_HD22	4.45	111.7
	L_O2···Thr127_HG1	4.70	110.5
	L_O1···Ser126_HG	4.21	98.0
	L_O1···Phe284_H	3.77	97.0
	L_O1···Asn325_HD21	4.87	121.5
	L_O1··· Asn325_HD22	4.87	10.8
	L_O5···Asn325_HD21	4.50	91.7
	L_O5···Asn325_HD22	4.50	31.8
	L_H22···Ser126_O[a]	2.72	127.6
	L_O6···Hip80_HD1	5.87	127.1
	L_O6···Leu81_H	5.08	112.4
	L_N5···Met78_H	3.64	70.8
	L_O7···Arg137_H11	3.59	111.8
	L_O7···Thr277_HG1	4.71	81.3
Complex F	L_O3···Gln92_HE21	4.30	62.67
	L_O3···Gln92_HE22	4.30	63.6
	L_O3···Ser319_HG	3.89	86.9
	L_O4···Ser319_HG	4.95	116.0
	L_O4···Gln119_HE21	3.15	73.1
	L_O4···Gln119_HE22	3.15	56.2
	L_O2···Thr127_HG1	4.41	83.4
	L_O1···Phe284_H	3.69	104.7
	L_O1···Ser126_HG[a]	2.88	92.4
	L_H22···Ser126_OG[a]	2.88	146.9
	L_H22···Asn325_OD1	4.71	149.9
	L_O5···Leu130_H	3.67	64.9
	L_N5···Met78_H	3.69	74.3
	L_O7···Met78_H	4.76	124.7

d(A···D) is the distance between the heavy atoms, and α(A···H–D) is the angle formed by the acceptor, hydrogen and donor atoms
L Ligand
[a]Indicates the regular H-bonds meeting the detection criteria

[27] and the root-mean-square distance (RMSD) between the initial and the final refined 3D model was 3.082. The model contains 322 amino acids. The following residues are involved in the TM regions: 39–65 (TM1 red), 75–102 (TM2 blue), 111–141 (TM3 yellow), 150–174 (TM4 violet), 198–224 (TM5 orange), 269–299 (TM6 cyan), and 309–332 (TM7 green) (Fig. 2), and a disulfide bridge is present between Cys112 and Cys187, as in all GPCRs [28].

In a previous publication [13], the hOTR used [11] was modeled using a δ-opioid template [29]. In the present study, the hOTR was homology modeled using the 3D structure of bRho, the generally accepted template [30, 31], determined via X-rays at high resolution (2.8 Å) [16].

The template used in this study is rather acceptable because this model was built up using a high-resolution crystal structure, while the previous hOTR was modeled by means of a theoretical template of the δ-opioid receptor, which do not contain the extracellular (EC) and intracellular (IC) loops. We made some comparisons between the two receptor models. After superimposing the two structures using the main-chain atoms, the RMSD was 7.903 (including 321 residues). After removal of the EC and IC loops from the models, the RMSD decreased to 3.442. These results allow the conclusion that the primary 3D model, based on the δ-opioid template, could also be used to study receptor–ligand interactions because the non-peptide ligands bind in the TM regions.

Using the filtration criteria, we obtained 18 possible structures from the 500 docked structures. These complexes were subjected to SA, the six structures with lowest energy were selected, and ΔG_{bind} was calculated by using the built-in scoring function of AutoDock 3.05 (Table 1).

The negative ΔG_{bind} values indicated that the refinement was successful after the rigid docking. For complexes A, C, and D, the morpholinone ring of the compound was located between the TM6 and TM7 regions, near the superficies of the receptor. This means that this part of the molecule could interact with the phospholipid bilayer, and these complexes were, therefore, excluded from further calculations.

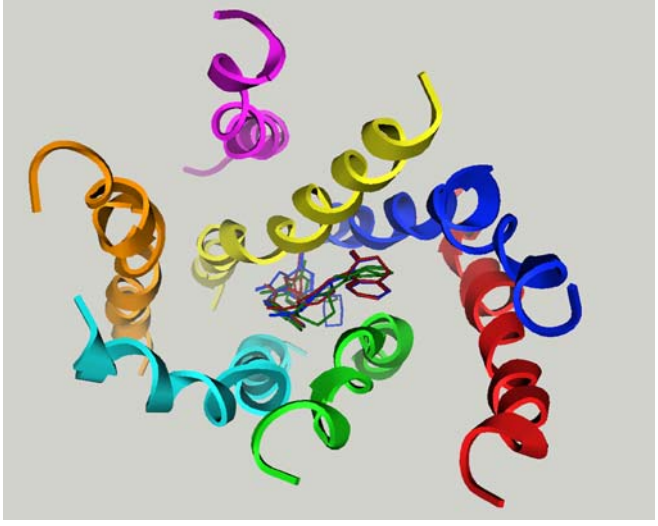

Fig. 3 The location of the ligands (complex B, *blue*; complex E, *red*; and complex F, *green*) in the transmembrane regions (TM1, *red*; TM2, *blue*; TM3, *yellow*; TM4, *purple*; TM5, *orange*; TM6, *cyan*; TM7, *green*) of the hOTR. For clarity, the EC and IC loops are not shown

For the remaining structures (complexes B, E, and F), the hydrophobic, H-bond and electrostatic interaction points were determined (Tables 2 and 3). Although the hydrophilic nature of the amino acids Asn and Gln could exclude them from hydrophobic interactions, the methylene group in the side-chain could interact with the hydrophobic part of the ligand; these residues were, therefore, identified as possible hydrophobic anchor points by LigPlot v4.4.2.

The H-bonds and possible electrostatic interactions are shown in Table 3. We accepted any electrostatic interaction as a regular H-bond when the distance between the acceptor atom and the donor atom (d(A···D)) was <3.2 Å [32] and the angle formed by the acceptor, hydrogen and donor atoms (α(A···H–D)) was >90 °. Residues closer than 4.5 Å to the possible anchor point in the ligand were taken into consideration, and all possible distances and angles were measured.

The important hydrophobic anchor point Ala318 was determined in each complex, which indicates that these complexes are possible active conformations. The ligands are located in the cleft formed by the regions TM2, 3, 6, and 7 (Fig. 3).

This finding is in good agreement with the fact that ligands of low molecular weight bind to sites within the hydrophobic core formed by the TM α-helices [33]. Among the hydrophobic interaction points, the possible electrostatic anchor points, including regular H-bonds, were also determined. In complex B one (L_O4···Met123_H), in complex E two (L_O4···Met123_H, L_H22···Ser126_O), and in complex F two (L_O1···Ser126_HG, L_H22···Ser126_OG), regular H-bonds were determined. Table 3 shows several interaction types that do not meet the detection criteria, but it must be borne in mind that these may change due to the dynamic behavior of the receptor–ligand complexes.

These results allow the conclusion that a stable complex could be formed through hydrophobic and electrostatic interactions. The alignment of the benzofuran part of the compound is maximal. The BZX part in complexes B and E is also superimposed. The only difference between these structures is the position of the amide group and the fact that the morpholinone ring is folded back. In complex F, the amide group is positioned in another orientation than in complex E; it, therefore, overlaps with the amide group of complex B. The orientation of the BZX ring in complex F is different from that in complexes B or E; it is rotated by 180 ° relative to the ring in the other two complexes (Fig. 4).

Independently of the orientation of the ligand, the possible anchor points are very similar in the complexes. As described above, the dynamic behavior of the receptor–ligand complexes means that the predefined anchor points can be changed; we, therefore, performed MD simulations on the three complexes.

In the MD simulations, we used neither membrane nor water (ε_r=1, constant dielectric constant [34]) with

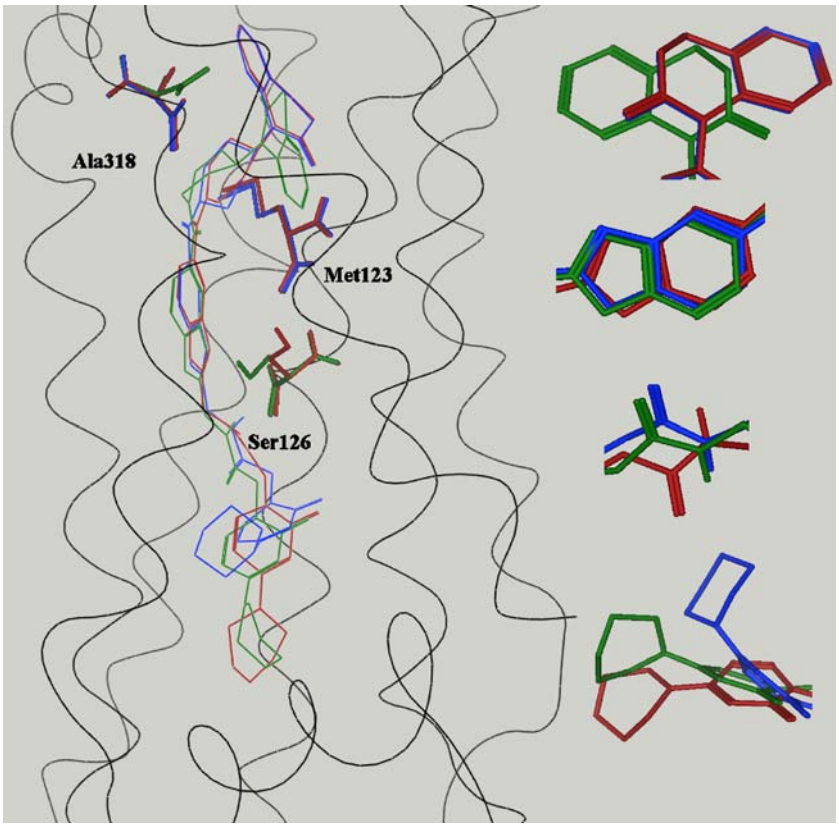

Fig. 4 The relative location of the ligands (complex B *blue*; complex E *red*; and complex *F* green) after the SA refinement. The important Ala318 residue, as hydrophobic contact point, is depicted with possible H-bond interaction points (Met123 and Ser126)

counterions. These options resulted in the following consequences: (1) without the membrane, we have to use positional restraints for the αC atoms in the TM regions to avoid helix degeneration or misfolding and (2) we used a distance-dependent dielectric constant to take the solvent screening effect (ε_r=4, water) into account. The reduced electrostatic interactions were, thus, mimicked, but it must be borne in mind that without the explicit water, the charged and polar surface residues (also in the binding site) can interact with each other and not with the solvent.

The plots of time vs root-mean-square distance (all-atom RMSD) for complexes B, E, and F are shown in Fig. 5.

Figure 5 shows that the RMSD did not change significantly during the last 1 ns, and we, therefore, analyzed only the last 1 ns trajectory for each complex.

We calculated ΔG_{bind} in the last 1 ns trajectory, taking every 50 ps frame for the calculation. The average energy values were as follows: −22.7±0.5, −23.0±0.3, and −23.3±0.5 for complexes B, E, and F, respectively. These values permit the statement that the MD simulation revealed that stable complexes could be formed, but these energy values did not facilitate a decision as to which complex could be used as a good basis for further assays or ligand design.

In each case, the hydrophobic (Table 4) and the previously determined possible electrostatic anchor point distances and angles were calculated every 1 ps (Table 5).

In each complex, the important residue (Ala318) is shown. Phe75, Gly122, and Thr277 hydrophobic contact points were found in major occurrence in complex F as compared with the other two complexes. The occurrence of Leu74, Phe77, Val88, Gln92, Ala283, and Ser319 was higher in complexes E and F than in complex B. In three cases, there was a major percentage occurrence in complex B (Leu129, Met135, and Ile328). These results indicate that, due to the hydrophobic effects, stable complexes can be formed in all cases.

Table 5 presents the possible electrostatic interactions. Only those interaction types are indicated where the percentage occurrence of the total electrostatic interaction

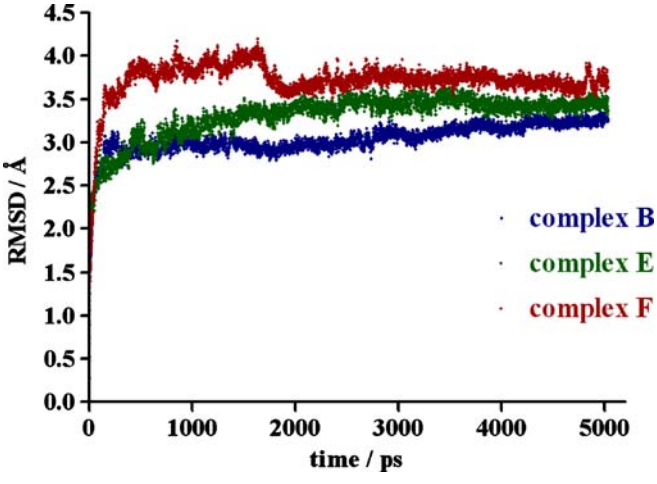

Fig. 5 Time vs RMSD plots for complexes B (*blue*), E (*green*), and F (*red*)

Table 4 Percentage occurrences of hydrophobic contact residues for complexes B, E, and F in the last 1-ns trajectory

	Occurrence (%)		
	Complex B	Complex E	Complex F
Leu74	0.0	51.2	87.4
Phe75	0.0	0.0	71.0
Phe77	17.2	41.2	46.5
Met78	**99.2**	**95.9**	**95.5**
Leu81	**99.8**	**95.3**	**86.1**
Val88	**0.0**	**83**	**100.0**
Gln92	29.2	100.0	93.9
Val93	0.0	10.9	5.3
Gln119	**100.0**	**100.0**	**95.1**
Gly122	0.0	0.0	82.1
Met123	**100.0**	**100.0**	**98.7**
Ser126	**100.0**	**100.0**	**100.0**
Thr127	99.5	99.1	94.2
Leu129	92.9	27	11.6
Leu130	**91.7**	**97.7**	**99.6**
Met133	**86.6**	**100.0**	**99.9**
Arg137	0.0	6.2	0.0
Phe185	11.6	5.6	0.0
Asp186	0.0	32.5	0.0
Trp188	21.1	0.0	0.0
Thr273	0.0	3.7	0.0
Met276	88.4	96.2	99.9
Thr277	1.8	1.7	84.7
Ile280	**100.0**	**100.0**	**100.0**
Ala283	19.3	50.1	89.0
Phe284	**100.0**	**100.0**	**100.0**
Cys287	**73.4**	**67.9**	**99.7**
Trp288	100.0	99.8	100.0
Phe291	17.1	0.0	0.0
Met315	44.5	0.0	0.0
Ala318	**100.0**	**100.0**	**98.2**
Ser319	**62.2**	**100.0**	**99.4**
Leu320	0.0	0.0	1.5
Asn321	**100.0**	**100.0**	**99.9**
Asn325	38.3	0.0	3.5
Ile328	87.2	0.0	0.0
Tyr329	54.7	0.0	99.7

The bold percentage values indicate those residues which were identified in the three static complexes (see Table 2)

exceeded 10%. We accepted the interaction type as an electrostatic interaction that could contribute to the complex stability when the heavy atom distances were <4 Å [32] and when the angle formed by the acceptor, hydrogen, and donor atoms was >90 °.

During the dynamics simulation, the electrostatic profiles of complexes B and F were largely rearranged.

After the SA in the case of complex B, six interactions met our H-bond or electrostatic criteria (L_O4⋯Gly122_H, L_O4⋯Met123_H, L_O4⋯Asn321_HD22, L_O1⋯Ser126_HG, L_O1⋯Phe284_H, and L_H22⋯Ser126_OG). After the MD simulation, only three cases met the criteria: L_O1⋯Ser126_HG, L_O1⋯Phe284_H, and a new interaction point, L_O3⋯Ser319_HG. For L_O1⋯Ser126_HG and L_O1⋯Phe284_H, the percentage occurrence was only 15.8 and 21.7%, respectively. For L_O3⋯Ser319_HG, a H-bond appeared in 50% of the structures.

In complex F, the electrostatic profile was changed to be very similar to complex B. After the SA, three interactions (L_O1⋯Phe284_H, L_O1⋯Ser126_HG, and L_H22⋯Ser126_OG) met the criteria. After the dynamics simulation, only L_O1⋯Ser126_HG was kept; the other three electrostatic interactions emerged in the dynamics simulation. We obtained H-bond interactions only in L_O4⋯Gln119_HE22.

Table 5 Calculated electrostatic interactions in complexes B, E, and F

Complex ID	Interacting atoms	d(A···D)/Å	α(A···H–D)/°	Occurrence of interaction (%)		
		Mean±SD	Mean±SD	H-bond	Electro	∑
Complex B	L_O3···Ser319_HG	3.24±0.48	98.2±33.0	45.0	14.9	59.9
	L_O1···Ser126_HG	4.12±0.18	89.4±19.6	0.0	15.8	15.8
	L_O1···Phe284_H	4.03±0.21	88.9±12.5	0.0	21.7	21.7
Complex E	L_O4···Gly122_H	3.91±0.17	102.7±6.8	0.0	71.3	71.3
	L_O4···Met123_H	3.17±0.16	99.1±12.6	44.8	31.0	75.8
	L_O1···Phe284_H	3.79±0.20	90.2±116	0.1	43.4	43.5
	L_H22···Ser126_O	2.87±0.12	122.4±12.8	99.1	0.7	99.8
	L_O7···Arg137_H11	3.68±0.29	114.0±15.6	5.1	75.9	81.0
Complex F	L_O4···Gln119_HE22	3.42±0.30	145.3±13.5	24.8	70.5	95.3
	L_O2···Thr127_HG1	4.22±0.23	99.3±11.9	0.0	12.5	12.5
	L_O1···Ser126_HG	3.87±0.32	98.9±23.7	0.2	54.1	54.3
	L_N5···Met78_H	3.47±0.15	79.0±9.9	0.9	13.8	14.7

d(A···D) is the distance between the two heavy atoms and α(A···H–D) is the angle formed by the acceptor, hydrogen, and donor atoms. We accepted an interaction as an electrostatic interaction when the heavy atom distances were <4 Å and as a H-bond when the heavy atom distances were <3.2 Å and when the angle formed by the acceptor, hydrogen and donor atoms was >90 °. The last three columns list the percent occurrence of the H-bond, only electrostatic (electro), and total electrostatic (∑) interactions

L Ligand

For complex E, a very different electrostatic profile was obtained. After the SA, five interactions were determined to be electrostatic interactions (L_O4···Gly122_H, L_O4··· Met123_H, L_O1···Phe284_H, L_H22···Ser126_O, and L_O7···Arg137_H11). During the MD simulation, these anchor points remained stable. This indicated that a more stable complex could occur for complex E as compared with B and F, as a result of hydrophobic and electrostatic interactions.

Comparison of the structures [SA (green), the last frame of the 5-ns trajectory (blue), and the average structure (red), which was calculated in the last 1 ns interval using heavy atoms and polar hydrogens) was also investigated (Fig. 6).

The variable region of the ligand in complex B remains in a stable conformation and location during the MD simulation. The BZX ring was moved from the initial position, which could be explained by the new electrostatic interaction point, Ser319. The Ala318 residue remained in the initial positions. In complex E, the ligand preserved its

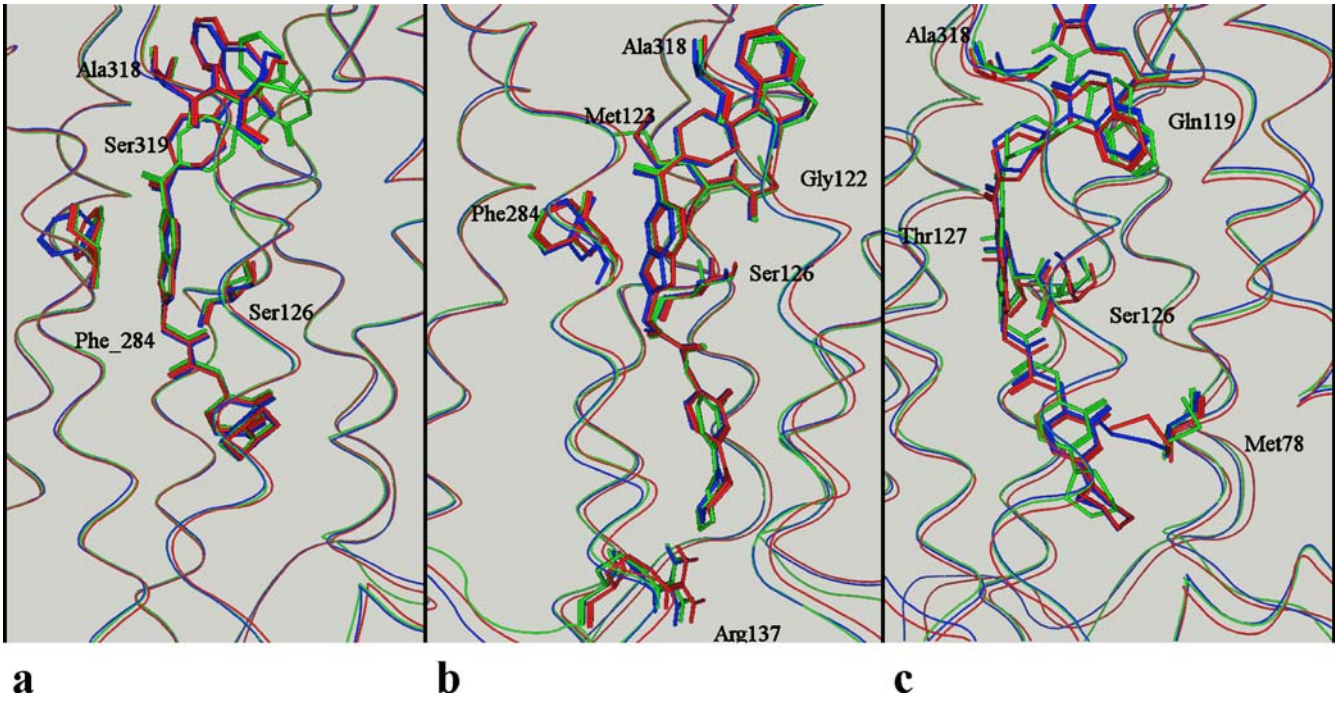

Fig. 6 Comparison of the structures obtained from SA (*green*), the last frame of the 5-ns trajectory (*blue*), and the average structure (*red*) in complexes B (**a**), E (**b**), and F (**c**)

initial location. Only for Met123 could a greater alteration in the side-chain conformation be detected between the depicted residues. The greatest alteration in the ligand was detected in complex F, and also in the side-chain location and position, with the exception of the Ala318 residue, which retained its initial location. A lower percentage of occurrence of Ala318 was observed in this complex (98.2%). As those structures were not followed by each other, where the Ala318 was not present as a hydrophobic contact point, this complex was not excluded from the potential active conformation. These findings also indicate that complex E is the most stable.

The fact that non-peptide ligands bind to the TM region of GPCRs [33] is in good agreement with the dynamic complex interaction sites. The hydrophobic (90–100% occurrence, Table 4) and the electrostatic (Table 5) interaction sites are located in the transmembrane region of the hOTR.

We conclude that complex E is a suitable active conformation; this could be confirmed by site-directed mutagenesis analyses. Although there is a great overlap of the hydrophobic and electrostatic interactions, we suggest that the Gly122 and Arg137 residues might be subjected to mutagenesis study. Residue Arg137 occurred as an electrostatic interaction point only in complex E. Residue Gly122 was determined in complex F to be a possible hydrophobic contact point, while in complex E it was determined to be a H-bond interaction site. The H-bond arose between the amide H and ligand (L_O4) but if this is replaced by a large-space-occupying residue (e.g., Phe), then no H-bond could be produced due to steric inhibition.

Summary and outlook

In the present study, we made an attempt to identify the key interaction elements of the dynamic hOTR–BZX complex. The 3D model building of hOTR was carried out with homology modeling using the bRho template. By means of molecular docking, filtration criteria (the presence of the Ala318 residue, as the most important interaction), and a refinement protocol (simulated annealing), we obtained three possible active conformations. To identify the most potential complex, a 5 ns MD simulation was performed, and determination of the hydrophobic and electrostatic interactions allowed the identification of the most likely conformation of the hOTR–BZX complex (complex E). These results could be supported via site-directed mutagenesis studies (Gly122 and Arg137), and the identified complex could be used in further calculations to support and improve our results.

Acknowledgements This work was supported by the Centenarium Foundation of Gedeon Richter and the National Council for Research and Technology (NKFP) Budapest (RET 08/2004).

Supplementary Material The 3D-coordinates of complex B, E and F in pdb format are available as supplementary material, together with the parameter topology file of BZX.

References

1. Cassoni P, Fulcheri E, Carcangiu ML, Stella A, Deaglio S, Bussolati G (2000) J Pathol 190:470–477
2. Thibonnier M, Conarty DM, Preston JA, Plesnicher CL, Dweik RA, Erzurum SC (1999) Endocrinology l140:1301–1309
3. Gutkowska J, Jankowski M, Lambert C, Mukaddam-Daher S, Zingg HH, McCann SM (1997) PNAS 94:11704–11709
4. Breton C, Haenggeli C, Barberis C, Heitz F, Bader CR, Bernheim L, Tribollet E (2002) J Clin Endocrinol Metab 87:1415–1418
5. Copland JA, Ives KL, Simmons DJ, Soloff MS (1999) Endocrinology 140:4371–4374
6. (2000) Pharm J 264:871 http://www.pjonline.com/Editorial/20000610/clinical/prematurebirth.html
7. Goodwin TM, Valenzuela G, Silver H, Hayashi R, Creasy GW, Lane R (1996) Am J Perinatol 13:143–149
8. Williams PD, Clineschmidt BV, Erb JM, Freidinger RM, Guidotti MT, Lis EV, Pawluczyk JM, Pettibone DJ, Reiss DR, Veber DF, Woyden CJ (1995) J Med Chem 38:4634–4636
9. Bell IB, Erb JM, Freidinger RM, Gallicchio SN, Guare JP, Guidotti MT, Halpin RA, Hobbs DW, Homnick CF, Kuo MS, Lis EV, Mathre DJ, Michelson SR, Pawluczyk JM, Pettibone DJ, Reiss DR, Vickers S, Williams PD, Woyden S (1998) J Med Chem 41:2146–2163
10. Kuo MS, Bock MG, Freidinger RM, Guidotti MT, Lis EV, Pawluczyk JM, Perlow DS, Pettibone DJ, Quigley AG, Reiss DR, Williams PD, Woyden CJ (1998) Bioorg Med Chem Lett 8:3081–3086
11. Giełdoń A, Kaźmierkiewicz R, Ślusarz R, Ciarkowski J (2002) J Comput Aided Mol Des 12:1085–1104
12. Hawtin SR, Ha SN, Pettibone DJ, Wheatley M (2005) FEBS Lett 579:349–356
13. Jójárt B, Martinek TA, Márki Á (2005) J Comput Aided Mol Des 19:341–356
14. Wyatt PG, Allen MJ, Chilcott J, Foster A, Livermore DG, Mordaunt JE, Scicinski J, Woollard P (2002) Bioorg Med Chem Lett 12:1399–1404
15. Wyatt PG, Allen MJ, Chilcott J, Gardner CJ, Livermore DG, Mordaunt JE, Nerozzi F, Patel M, Perren MJ, Weingarten GG, Shabbir S, Wollard PM, Zhou P (2002) Bioorg Med Chem Lett 12:1405–1411
16. Palczewski K, Kumasaka T, Hori T, Behnke CA, Motoshima H, Fox BA, Le Trong I, Teller DC, Okada T, Stenkamp RE, Yamamoto M, Miyano M (2000) Science 289:739–745
17. Molecular Operating Environment (MOE 2004.03). CCG, 1255 University St, Suite 1600, Montreal, Quebec, Canada, H3B3X3
18. Cornell WD, Cieplak P, Bayly CI, Gould IR, Merz KM Jr, Ferguson DM, Spellmeyer DC, Fox T, Caldwell JW, Kollman PA (1995) J Am Chem Soc 117:5179–5197
19. Case DA, Darden TA, Cheatham TE, III, Simmerling CL, Wang J, Duke RE, Luo R, Merz KM, Wang B, Pearlman DA, Crowley M, Brozell S, Tsui V, Gohlke H, Mongan J, Hornak V, Cui G, Beroza P, Schafmeister C, Caldwell JW, Ross WS, Kollman PA (2004) AMBER 8, University of California, San Francisco
20. Morris GM, Goodsell DS, Halliday RS, Huey R, Hart WE, Belew RK, Olson AJ (1998) J Comput Chem 19:1639–1662
21. Halgren TA (1996) J Comput Chem 17:490–519, 520–552, 553–586, 587–615, 616–641
22. Mehler EL, Solmajer T (1991) Protein Eng 4:903−910
23. Wallace AC, Laskowski RA, Thornton JM (1995) Protein Eng 8:127–134
24. Wang J, Wolf RM, Caldwell JW, Kollman PA, Case DA (2004) J Comput Chem 25:1157–1174
25. Zaffran T, Cieplak P, Dupradeau F-Y (2005) RESP ESP charge Derive (RED) II. The Scripps Research Institute, La Jolla, CA, USA

26. Frisch MJ, Trucks GW, Schlegel HB, Scuseria GE, Robb MA, Cheeseman JR, Montgomery JA, Jr, Vreven T, Kudin KN, Burant JC, Millam lM, Iyengar SS, Tomasi J, Barone V, Mennucci B, Cossi M, Scalmani G, Rega N, Petersson G A, Nakatsuji H, Hada M, Ehara M, Toyota K, Fukuda R, Hasegawa J, Ishida M, Nakajima T, Honda Y, Kitao O, Nakai H, Klene M, Li X, Knox JE, Hratchian HP, Cross JB, Adamo C, Jaramillo J, Gomperts R, Stratmann RE, Yazyev O, Austin AJ, Cammi R, Pomelli C, Ochterski JW, Ayala PY, Morokuma K, Voth GA, Salvador P, Dannenberg JJ, Zakrzewski VG, Dapprich S, Daniels AD, Strain MC, Farkas O, Malick DK, Rabuck AD, Raghavachari K, Foresman JB, Ortiz JV, Cui Q, Baboul AG, Clifford S, Cioslowski J, Stefanov BB, Liu G, Liashenko A, Piskorz P, Komaromi I, Martin RL, Fox DJ, Keith T, Al-Laham MA, Peng, Nanayakkara A, Challacombe M, Gill PMW, Johnson B, Cen W, Wong MW, Gonzalez C, Pople JA (2003) Gaussian 03, revision B01. Gaussian, Pittsburgh, PA
27. Laskowski RA, Moss AS, Thornton JM (1993) J Mol Biol 231:1049–1067
28. Gether U (2000) Endocr Rev 21:90–113
29. Pogozheva ID, Lomize AL, Mosberg HI (1998) Biophys J 75:612–634
30. Archer E, Maigret B, Escrieut C, Pradayrol L, Fourmy D (2003) TIPS 24:36–40
31. Moro S, Spalluto G, Jacobson KA (2005) TIPS 26:44–50
32. Fernandez JH, Neshich G, Camargo1 ACM (2004) Genet Mol Res 4:554–563
33. Gether U, Kobilka BK (1998) J Biol Chem l273:17979–17982
34. Śluzarz MJ, Giełdoñ A, Ślusarz R, Trojnar J, Meadows R, Ciarkowski J (2005) QSAR Comb Sci 24:603–610